

# Exact results of the limited penetrable horizontal visibility graph associated to random time series and its application

Minggang Wang,<sup>1,2,3,\*</sup> André L.M.Vilela,<sup>3,4</sup> Ruijin Du,<sup>3,5</sup> Longfeng Zhao,<sup>3</sup> Gaogao Dong,<sup>3,5</sup> Lixin Tian,<sup>1,5,†</sup> and H. Eugene Stanley<sup>3</sup>

<sup>1</sup>*School of Mathematical Science, Nanjing Normal University, Nanjing 210042, Jiangsu, China*

<sup>2</sup>*Department of Mathematics, Nanjing Normal University Taizhou College, Taizhou 225300, Jiangsu, China*

<sup>3</sup>*Center for Polymer Studies and Department of Physics, Boston University, Boston, MA 02215, USA*

<sup>4</sup>*Universidade de Pernambuco, 50720-001, Recife-PE, Brazil*

<sup>5</sup>*Energy Development and Environmental Protection Strategy Research Center, Jiangsu University, Zhenjiang, 212013 Jiangsu, China*

The limited penetrable horizontal visibility algorithm is a new time analysis tool and is a further development of the horizontal visibility algorithm. We present some exact results on the topological properties of the limited penetrable horizontal visibility graph associated with random series. We show that the random series maps on a limited penetrable horizontal visibility graph with exponential degree distribution  $P(k) \sim \exp[-\lambda(k - 2\rho - 2)]$ ,  $\lambda = \ln[(2\rho + 3)/(2\rho + 2)]$ ,  $\rho = 0, 1, 2, \dots$ ,  $k = 2\rho + 2, 2\rho + 3, \dots$ , independent of the probability distribution from which the series was generated. We deduce the exact expressions of the mean degree and the clustering coefficient and demonstrate the long distance visibility property. Numerical simulations confirm the accuracy of our theoretical results. We then examine several deterministic chaotic series (a logistic map, the Hénon map, the Lorenz system, and an energy price chaotic system) and a real crude oil price series to test our results. The empirical results show that the limited penetrable horizontal visibility algorithm is direct, has a low computational cost when discriminating chaos from uncorrelated randomness, and is able to measure the global evolution characteristics of the real time series.

PACS numbers: 05.45. Tp, 89.75. Hc, 05.45.-a

## I. INTRODUCTION

Several methodologies for understanding the complicated behavior of nonlinear time series have been recently developed, including chaos analysis [1], fractal analysis [2], and complexity measurement [3]. With the development of complex network theories [4–7], a new multidisciplinary methodology for characterizing nonlinear time series using complex network science has emerged and rapidly expanded [8–24]. The main tool of these methods is to use an algorithm or algorithms to transform a nonlinear time series into a corresponding complex network and then use the topological structure of complex networks to analyze the properties of the nonlinear time series.

Currently there are four ways of converting univariate time series into complex networks. The first one is Pseudo-periodic time series transitions [8] that analyze pseudo-periodic time series. The second one is the visibility graph (VG) method, which

---

\*Electronic address: magic821204@sina.com;magic82@bu.edu

†Electronic address: tianlx@ujs.edu.cn

was first proposed by Lacasa et al. [9–10]. To facilitate computation, Luque et al. [11–12] proposed a simplified horizontal visibility algorithm (HVG) based on the visibility algorithm. Bezsudnov et al. [13] proposed a parameter visibility method. Gao et al. [14] proposed a limited penetrable visibility method (LPVG) and multiscale limited penetrable horizontal visibility graph (MLPHVG). The third one is the phase space reconstruction method [15–16]. It begins with a phase space reconstruction of time series analysis, maps fixed-length time series segments into nodes of a network, and then uses the correlation coefficients (or distances) between these nodes to determine whether they are connected or not. And the last one is the coarse graining method [17–20] by which fluctuations of time series are transformed into signal sequences. A fixed-length signal sequence is treated as a network node that connects nodes of time series in chronological order, and a weighted complex network with direction is then constructed. In recent years, researchers have used complex network theories to study multivariate time series [21–24]. These four methods all effectively maintain most of the properties of different types of time series, and they have been successfully used in many different fields [25–30].

Although there have been abundant empirical results obtained using time series complex network algorithms [8–24], rigorous theoretical results are still lacking. Only a small amount of literature [9–12] has presented exact results on the properties of the horizontal visibility graphs (HVG) associated with random series. Thus far no rigorous theory other than the above algorithms has been developed. Thus our goal here is to focus on one type of general horizontal visibility algorithm, the limited penetrable horizontal visibility graph (LPHVG), and derive exact results on the properties of the limited penetrable horizontal visibility graphs associated with random series. We prove that an independent and identically distributed random series can be mapped on a limited penetrable horizontal visibility graph with exponential degree distribution  $P(k) \sim \exp[-\lambda(k - 2\rho - 2)]$ ,  $\lambda = \ln[(2\rho + 3)/(2\rho + 2)]$ ,  $\rho = 0, 1, 2, \dots, k = 2\rho + 2, 2\rho + 3, \dots$ , which is an extension of the result presented in Ref. [11]. We deduce the exact mean degree and the clustering coefficient, and we prove that the limited penetrable horizontal visibility graph associated with any independent and identically distributed random series has a small world characteristic. To verify our theoretical solution, we acquire simulation results by using several deterministic chaotic series (a logistic map, an Hénon map, the Lorentz system, and the energy price chaos system) and a real-world crude oil price series that confirms the accuracy and usability of our exact results.

## II. RESULTS

We here supply several exact results of LPHVG associated with random time series and apply them to several deterministic chaotic series (a logistic map, an Hénon map, the Lorentz system, and the energy price chaos system) and a real-world crude oil price series.

**Degree distribution.** Let  $X(t)$  be a real valued bi-infinite time series of independent and identically distributed (*i.i.d.*) random variables with a probability density  $f(x)$  in which  $x \in [a, b]$ , and consider its associated LPHVG with the limited penetrable distance  $\rho = 1$ . Then

$$P(k) \sim \exp[-(k - 4)\ln(5/4)], k = 4, 5, \dots, \forall f(x). \quad (1)$$

To prove this conclusion we first calculate the probability that an arbitrary datum with value  $x_0$  has a limited penetrability at most a one-time visibility of  $k$  other data. We thus list all sets of possible configurations for data  $x_0$  with  $k = 4$  (see Fig. S1 in Appendix),  $k = 5$  (see Fig. S2 in Appendix), and  $k = 6$  (see Fig. S3 in Appendix), and we calculate the probability  $P(k = 4)$  (see Eq. (S4)),  $P(k = 5)$  (see Eq. (S9)), and  $P(k = 6)$  (see Eq. (S10)). We then deduce the rules of when a given

configuration contributes to  $P(k)$  (see rules i–iv) and obtain a general expression for  $P(k)$  (see Eq. (S12)). The detailed proof of this result is shown in *Appendix Theorem S1*. This is an exact result for a limited penetrable horizontal visibility graph with the limited penetrable distance  $\rho = 1$ . We conclude that for every probability distribution  $f(x)$ , the degree distribution  $P(k)$  of the associated LPHVG has the same exponential form. In addition, from this result we can obtain the more general result (*Theorem S2 in Appendix*) in which  $X(t)$  is a real bi-infinite time series of *i.i.d.* random variables with a probability distribution  $f(x)$  in which  $x \in [a, b]$ , and can examine its associated LPHVG with the limited penetrable distance  $\rho$ . Then

$$P(k) \sim \exp\{-(k - 2\rho - 2)\ln[(2\rho + 3)/(2\rho + 2)]\}, \rho = 0, 1, 2, \dots, k = 2\rho + 2, 2\rho + 3, \dots, \forall f(x). \quad (2)$$

Note that when  $\rho = 0$ , then  $P(k) \sim \exp[-(k - 2)\ln(3/2)]$ , the result in Ref. [11]. In fact, when  $\rho = 0$  the LPHVG becomes the HVG (see *Methods Section*). When  $\rho = 1$ , the result is Eq. (1). Therefore Eq. (2) is an extension of the previous result [11] that indicates that the degree distribution  $P(k)$  of LPHVG associated with *i.i.d.* random time series has a unified exponential form.

To further check the accuracy of our analytical results, we perform several numerical simulations. We generate a random series of 3000 data points from uniform, gaussian, and power law distributions and their associated limited penetrable horizontal visibility graphs. Figs 1(a) and 1(b) show plots of the degree distributions of the resulting graphs with a penetrable distance  $\rho = 1$  and  $\rho = 2$ . Here circles indicate a series extracted from a uniform distribution, and squares and diamonds indicate series extracted from gaussian and power law distributions, respectively. The solid line indicates the theoretical results of Eq. (2). We find that the theoretical results agree with the numerics. Note that a prerequisite for our theoretical results is that the length of the time series must be infinitely long, i.e. the series size  $N \rightarrow \infty$ , so we can assert that the tail degree distribution of LPHVG associated to *i.i.d.* random series deviated from the theoretical result is only due to the effect of the finite size. In order to check the effect of the finite size, we define the relative error ( $E(k)$ ) and the mean relative error ( $ME$ ) to measure accurate between the numerical result under the finite size and the theoretical result, and use a cutoff value  $k_0$  to denote the onset of finite size effects.

$$E(k) = \frac{|P_{num}(k) - P_{the}(k)|}{P_{the}(k)}, ME = \sum_k E(k) \quad (3)$$

where,  $P_{num}(k)$  and  $P_{the}(k)$  represent the degree distribution of the numerical result and theoretical result respectively. We generate the random series from uniform distribution with different the series size. We have generated 10 realizations of each series size  $N$ . Fig. 1 (c) shows the test results of the resulting graphs with penetrable distance  $\rho = 1$  and Fig. 1 (d) shows the test results of the resulting graphs with penetrable distance  $\rho = 2$ . The subplots in Figs. 1 (c) and (d) show the relations between the mean relative error ( $ME$ ) and the series size  $N$ , and the relations between the cutoff value  $k_0$  and the series size  $N$ . We find that the the mean relative error ( $ME$ ) decreases with the finite size  $N$  increases, and the cutoff value  $k_0$  increases with the finite size  $N$  increases, which agreement with our previous assertion.

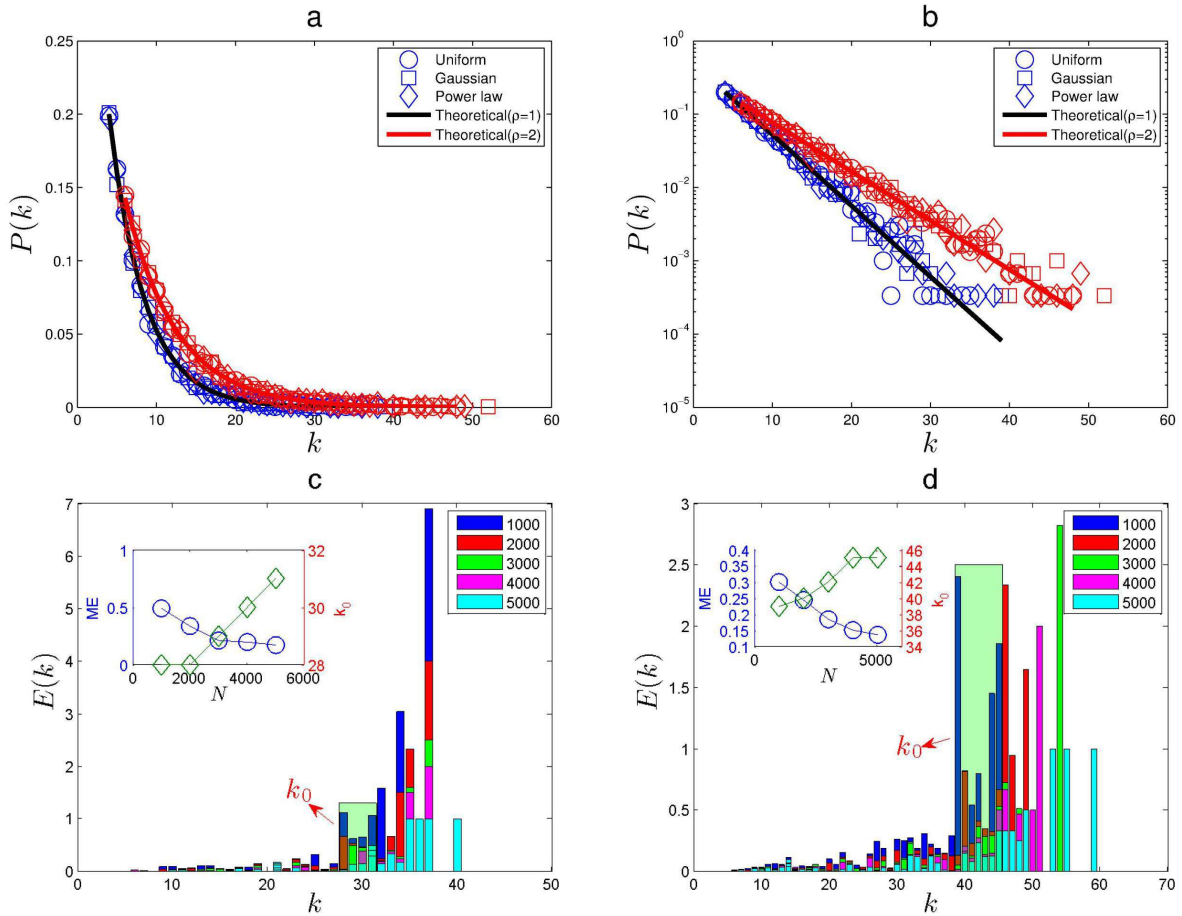


FIG. 1: (a) Plot of the degree distribution of the resulting graphs with penetrable distance  $\rho = 1$  and  $\rho = 2$ , (b) semi-log plot of the degree distribution of the resulting graphs with penetrable distance  $\rho = 1$  and  $\rho = 2$ , (c) the test results of the resulting graphs with penetrable distance  $\rho = 1$  (ensemble averaged over 10 realizations), (d) the test results of the resulting graphs with penetrable distance  $\rho = 2$  (ensemble averaged over 10 realizations)

**Mean degree.** Using Eq. (2) we calculate the mean degree  $\langle k \rangle$  of the LPHVG associated with an uncorrelated random series,

$$\langle k \rangle = \sum_k k P(k) = \sum_{k=2(\rho+1)}^{\infty} \frac{k}{2\rho+3} \left(\frac{2\rho+2}{2\rho+3}\right)^{k-2(\rho+1)} = 4(\rho+1). \quad (4)$$

We next deduce the more general expression of mean degree  $\langle k(T) \rangle$ . We consider an infinite periodic series of period  $T$  (with no repeated values in a period) denoted  $X_t = \{\dots, x_0, x_1, x_2, \dots, x_T, x_1, x_2, \dots\}$ , where  $x_0 = x_T$ . Let  $\rho \ll T$  for the subseries  $\tilde{X}_t = \{x_0, x_1, x_2, \dots, x_T\}$ . Without losing generality, we assume  $x_0 = x_T$  corresponds to the largest value of the subseries, and  $x_1, \dots, x_\rho, x_{T-\rho}, \dots, x_{T-1}$  corresponds to the  $(2\rho+1)$ nd largest value of the subseries. We then can construct the LPHVG associated with the subseries  $\tilde{X}_t$ . If the LPHVG has  $E$  links and  $x_i$  is smallest datum of  $\tilde{X}_t$ , because no data repetitions are allowed in  $\tilde{X}_t$ , the degree of  $x_i$  is  $2(\rho+1)$  during the construction of LPHVG, when  $\rho = 1$ , see Fig. S1. We delete node  $x_i$  and its  $2(\rho+1)$  links from the LPHVG. The resulting graph has  $E - 2(\rho+1)$  links and  $T$  nodes. We iterate this process

$T - (2\rho + 1)$  times (see Fig. 2 for a graphical illustration of this process in the case  $\rho = 1, T = 10$ ), and the total number of deleted links is now  $E_d = 2(\rho + 1)[T - (2\rho + 1)]$ . The resulting graph has  $2(\rho + 1)$  nodes, i.e.,  $x_0, x_1, \dots, x_\rho, x_{T-\rho}, \dots, x_{T-1}, x_T$ , see Fig. 2(h) for  $\rho = 1$  and  $T = 10$ . Because these  $2(\rho + 1)$  nodes are connected by  $E_r = \binom{2(\rho+1)}{2}$  links, the mean degree of a limited penetrable horizontal visibility graph associated with  $X_t$  is

$$\langle k(T) \rangle = 2 \frac{E_d + E_r}{T} = \frac{2[(2(\rho + 1))(T - (2\rho + 1)) + (\rho + 1)(2\rho + 1)]}{T} = 4(\rho + 1) \left(1 - \frac{2\rho + 1}{2T}\right), \rho \ll T. \quad (5)$$

Note that Eq. (5) holds for every periodic or aperiodic series in which  $T \rightarrow \infty$ , independent of the deterministic process that generates the series. This is the case because the only constraint in its derivation is that data within a period are not repeated. Note that one consequence of Eq. (5) is that every time series has an associated LPHVG with the maximum mean degree (achieved for aperiodic series)  $\langle k(\infty) \rangle = 4(\rho + 1)$ , which agrees with Eq. (4).

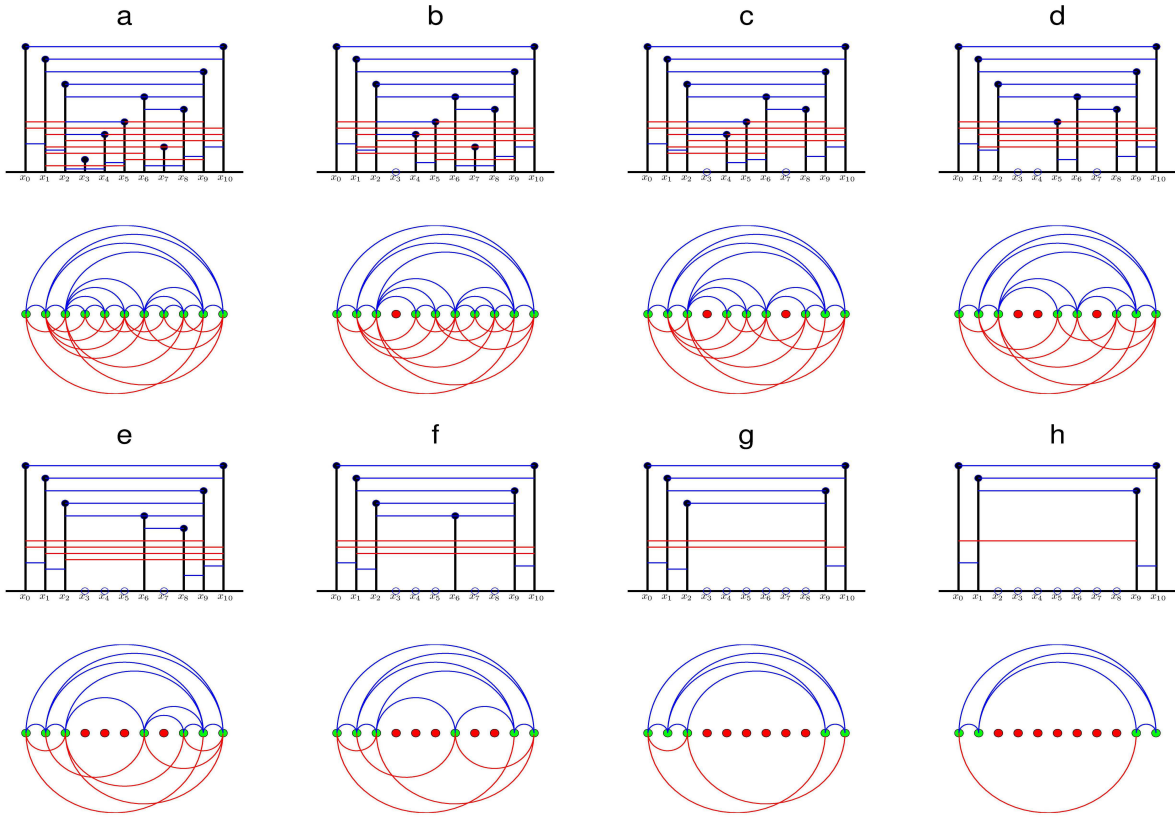


FIG. 2: Graphical illustration of the constructive proof of  $\langle k(T) \rangle$ , considering a LPHVG with  $\rho = 1$  extracted from a periodic series of period  $T = 10$ .

To check the accuracy of our analytical result, we generate simple period-50, period-100, period-200, and period-250 time series with 1000 data points [see Fig. 3(a)]. We construct the limited penetrable horizontal visibility graphs with the penetrable distance  $\rho = 0, 1, 2, \dots, 10$  associated with this periodic time series. Fig. 3(b) shows a plot of the mean degree of the resulting LPHVGs with different  $\rho$  values, and there is an excellent agreement with the numerics  $\rho \ll T$ .

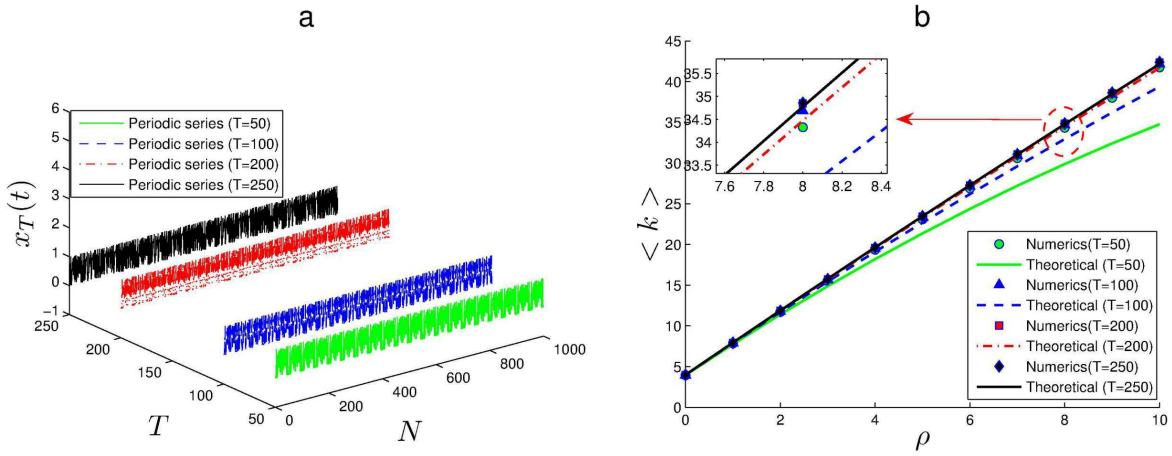


FIG. 3: (a) A simplified period-50, period-100, period-200 and period-250 time series of 1000 data, (b) plotted the mean degree of the resulting LPHVGs with different  $\rho$  (circles correspond to the periodic-50, triangles correspond to the periodic-100, squares correspond to the periodic-200 and diamonds correspond to the periodic-250 time series, the black, blue, red and green solid line correspond to the theoretical result respectively).

**Local clustering coefficient.** In LPHVG, a given nodes with the same degree usual have the different clustering coefficients since the degree of the node contributed by the different configurations which have different structures (see the proof process of Theorem S1). By calculating the clustering coefficients of different configurations (see Theorem S3), we find that the clustering coefficients of the nodes in LPHVG are irregular, but the minimum clustering coefficient and the maximum clustering coefficient of these nodes are regular. Therefore, Based on the results of degree distribution [Eq. (2)], we can deduce the minimum local clustering coefficient  $C_{min}(k)$  and the maximum clustering coefficient  $C_{max}(k)$  of LPHVG associated to *i.i.d.* random series by the following expression,

$$C_{min}(k) = \frac{2}{k} + \frac{2\rho(k-2)}{k(k-1)}, \rho = 0, 1, 2, k \geq 2(\rho + 1), \quad (6)$$

$$C_{max}(k) = \frac{2}{k} + \frac{4\rho(k-3)}{k(k-1)}, \rho = 0, 1, 2, k \geq 2(2\rho + 1). \quad (7)$$

Using Eqs. (2), (6), and (7) we also obtain the local clustering coefficient distribution  $P(C_{min})$  and  $P(C_{max})$ , i.e.,

$$P(C_{min}) = \frac{1}{2\rho+3} \exp\left\{\left[\frac{\varphi + \sqrt{\varphi^2 - 8C_{min}(2\rho+1)}}{2C_{min}} - 2(\rho+1)\right] \ln\left(\frac{2\rho+2}{2\rho+3}\right)\right\}, \varphi = C_{min} + 2\rho + 2, \quad (8)$$

$$P(C_{max}) = \frac{1}{2\rho+3} \exp\left\{\left[\frac{\phi + \sqrt{\phi^2 - 8C_{max}(6\rho+1)}}{2C_{max}} - 2(\rho+1)\right] \ln\left(\frac{2\rho+2}{2\rho+3}\right)\right\}, \phi = C_{max} + 4\rho + 2. \quad (9)$$

For a proof of this result see Theorem S3 in the Appendix. Fig. 4 shows the clustering coefficient  $C_k$  and the clustering coefficient distribution  $P(C)$  of limited penetrable horizontal visibility graphs associated with different random series of 3000 data points obtained numerically. The solid black line in Figs. 4(a) and 4(b) is the theoretical prediction of  $C_{min}(k)$  [see Eq. (6)], and the solid red line is the theoretical prediction of  $C_{max}(k)$  [see Eq. (7)]. The solid black line in Figs. 4(c) and 4(d) is the theoretical

prediction of  $P(C_{\min})$  [see Eq. (8)], and the solid red line is the theoretical prediction of  $P(C_{\max})$  [see Eq. (9)]. Fig. 4 shows that the theoretical predictions of  $C_{\min}(k)$ ,  $C_{\max}(k)$ ,  $P(C_{\min})$ , and  $P(C_{\max})$  agree with the numerics.

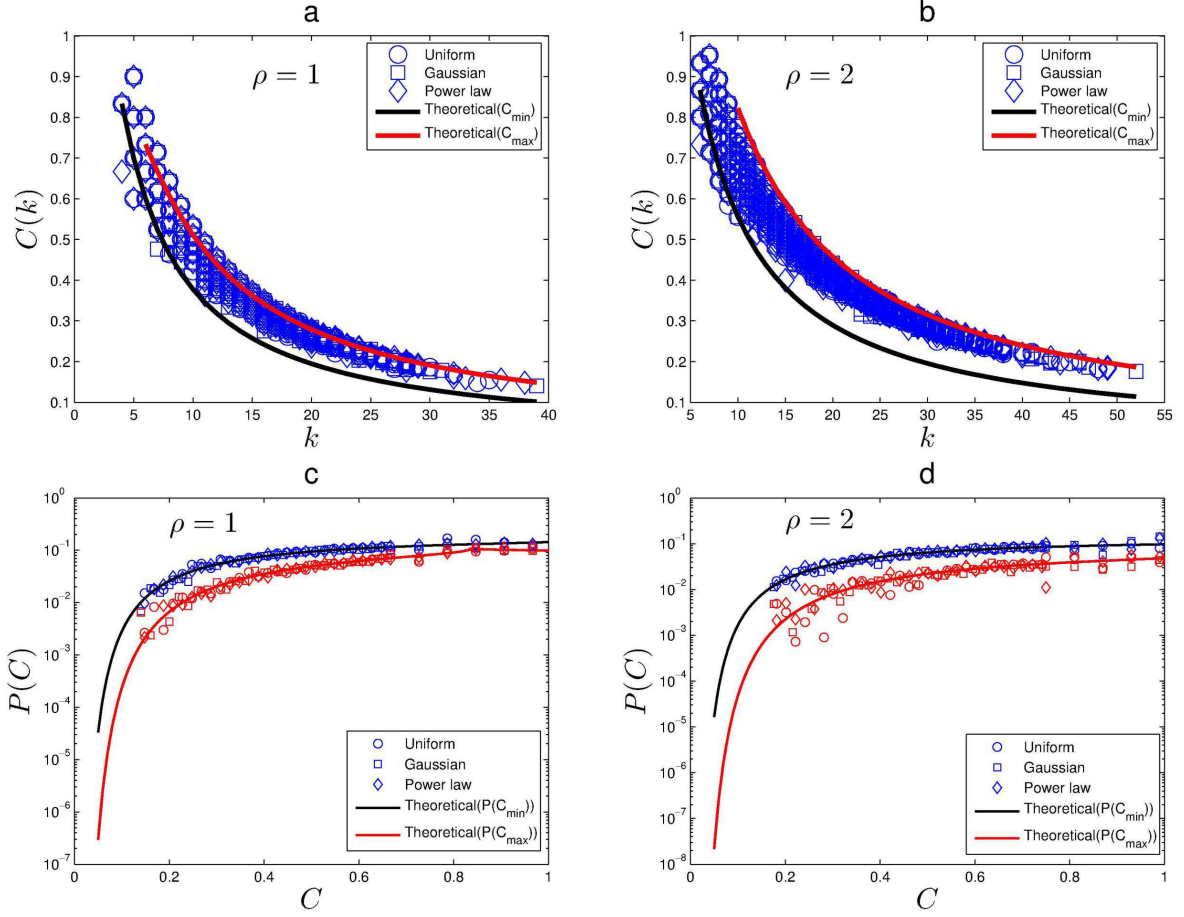


FIG. 4: The relationship between degree and clustering coefficient of LPHVG (a)  $\rho = 1$ , (b)  $\rho = 2$ . The solid black line corresponds to the theoretical prediction of  $C_{\min}(k)$  [Eq.(6)], the solid red line corresponds to the theoretical prediction of  $C_{\max}(k)$  [Eq. (7)]. The clustering coefficient distribution (c)  $\rho = 1$ , (d)  $\rho = 2$ . The solid black line corresponds to the theoretical prediction of  $P(C_{\min})$  [Eq. (8)], the solid red line corresponds to the theoretical prediction of  $P(C_{\max})$  [Eq. (9)].

**Long distance visibility.** In a limited penetrable horizontal visibility graph associated with a bi-finite sequence of *i.i.d.* random variables extracted from a continuous probability density  $f(x)$ , the probability  $P_\rho(n)$  that two data points separated by  $n$  intermediate data points are connected is

$$P_\rho(n) = \frac{2\rho(\rho + 1) + 2}{n(n + 1)}. \quad (10)$$

Note that  $P_\rho(n)$  is again independent of the probability distribution of the random variable  $X$ . For a detailed proof of this result see Theorem S4 in the Appendix. Fig. 5(a) shows the adjacency matrix  $\mathbf{A}$  of the limited penetrable horizontal visibility graph associated with a random series with a different limited penetrable distance. When  $A(i, j) = 1$ , we plot  $\rho = 0$  (circle),  $\rho = 1$  (triangle),  $\rho = 2$  (square), and  $\rho = 3$  (diamond) at  $(i, \rho, j)$  and  $(j, \rho, i)$ .

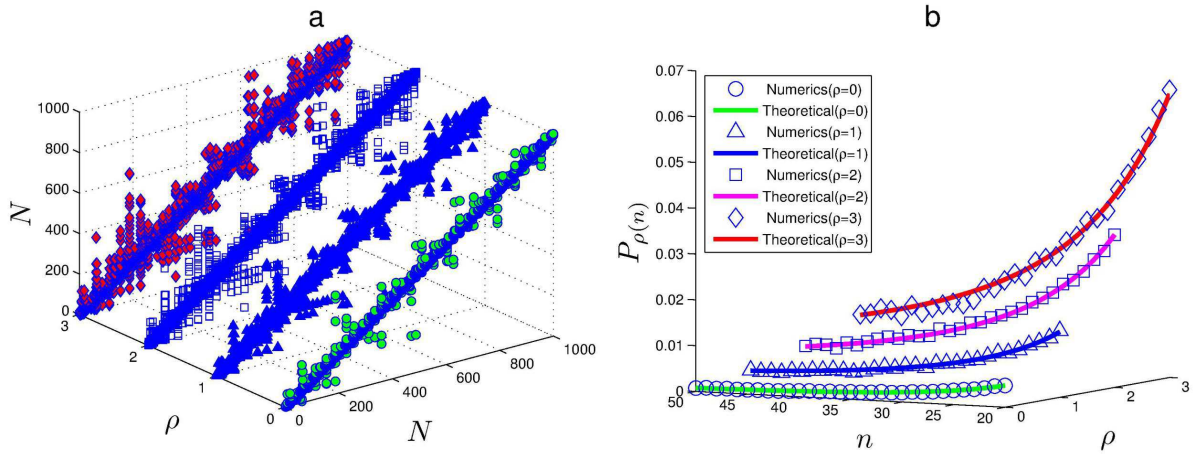


FIG. 5: (a) Adjacency matrix of LPHVG associated to a random series with different  $\rho$ , (b) plot of the relationship of  $\rho, n$  and  $P_\rho(n)$  (the solid line correspond to the theoretical result [Eq. (10)], circles correspond to the numerical simulation result for  $\rho = 0$ , triangles correspond to the numerical simulation result for  $\rho = 1$ , squares correspond to the numerical simulation result for  $\rho = 2$ , diamond correspond to the numerical simulation result for  $\rho = 3$ ).

Fig. 5(a) shows a typical homogeneous structure in which the adjacency matrix is filled around the main diagonal. In addition, the matrix indicates a superposed sparse structure caused by the limited penetrable visibility probability  $P_\rho(n) = \frac{2\rho(\rho+1)+2}{n(n+1)}$  that introduces shortcuts into the limited penetrable horizontal visibility graph. These shortcuts indicate that the limited penetrable horizontal visibility graph is a small-world phenomenon. Fig. 5(b) shows that the theoretical result in Eq. (10) agrees with the numerics.

These results are exact with regard to the topological properties of the limited penetrable horizontal visibility graphs associated with *i.i.d.* random series via the limited penetrable horizontal visibility algorithm.

**Application to deterministic chaotic time series.** These results can be used to discriminate between random and chaotic signals. Because stochastic and chaotic processes share many features, discriminating between them is difficult, and methods of identifying random processes and discriminating between deterministic chaotic systems and stochastic processes has received extensive study in recent decades [31–34]. Most previous algorithms have been phenomenological and computationally complicated. Thus new methods that can reliably distinguish stochastic from chaotic time series are needed. Recently Lacasa et al. [11–12] used the horizontal visibility algorithm to characterize and distinguish between stochastic and chaotic processes, and they demonstrated that it could easily distinguish chaotic from random series. Here we use our new theory to distinguish chaotic series from random series and compare with the horizontal visibility algorithm [11], and we address four deterministic time series generated by the Logistic map [35]

$$x_{t+1} = \mu x_t(1 - x_t), \mu = 4,$$

the Hénon map [36],

$$x_{t+1} = 1 + y_t - ax_t^2, y_{t+1} = bx_t, a = 1.4, b = 0.3,$$



the Lorenz chaos system [37],

$$\dot{x} = a(y - x), \dot{y} = cx - y - xz, \dot{z} = xy - bz, a = 10, b = 8/3, c = 28,$$

and the energy price-supply-economic growth system [27],  $\dot{x} = a_1x + a_2(C - y) + a_3(z - K_1)$ ,  $\dot{y} = -b_1y + b_2x - b_3z(1 - z/K_2)$ ,  $\dot{z} = c_1z(1 - z/L) + C_2yza_1 = 0.3, C = 27, a_2 = 0.5563, a_3 = 0.15, b_1 = 0.4, b_2 = 0.6073, b_3 = 0.3, K_1 = 15, K_2 = 15, c_1 = 0.3, c_2 = 0.006, L = 19$ .

Fig. 6 shows the limited penetrable horizontal visibility graphs of 3000 data points extracted from two different chaotic maps and two different chaotic system with  $\rho = 0$  to the left,  $\rho = 1$  in the middle, and  $\rho = 2$  to the right. We calculate their degree distribution numerically (top panel) and the relationship between degree and clustering coefficient (bottom panel). In every case  $P(k)$  deviates from Eq. (2) and  $C(k)$  deviates from Eqs. (6) and (7). We also find that the degree distributions of the LPHVGs associated with these chaotic maps and chaotic systems can be approximated using the exponential function  $P(k) \sim \exp(-\hat{\lambda})k$ , but  $\hat{\lambda} \neq \lambda = \ln[(2\rho+3)/(2\rho+2)]$  in each case, and we conjecture that there is a functional relationship between the random and chaos dimensions [11]. Thus the parameter  $\lambda = \ln[(2\rho+3)/(2\rho+2)]$  is the frontier between random series and chaotic series and serves to distinguish randomness from chaos. Fig. 6 shows (bottom panel) that the limited penetrable horizontal visibility graphs of  $\rho = 1$  in the middle and  $\rho = 2$  on the right serve as better discriminators from the perspective of  $C(k)$  than the horizontal visibility graph of  $\rho = 0$  on the left.

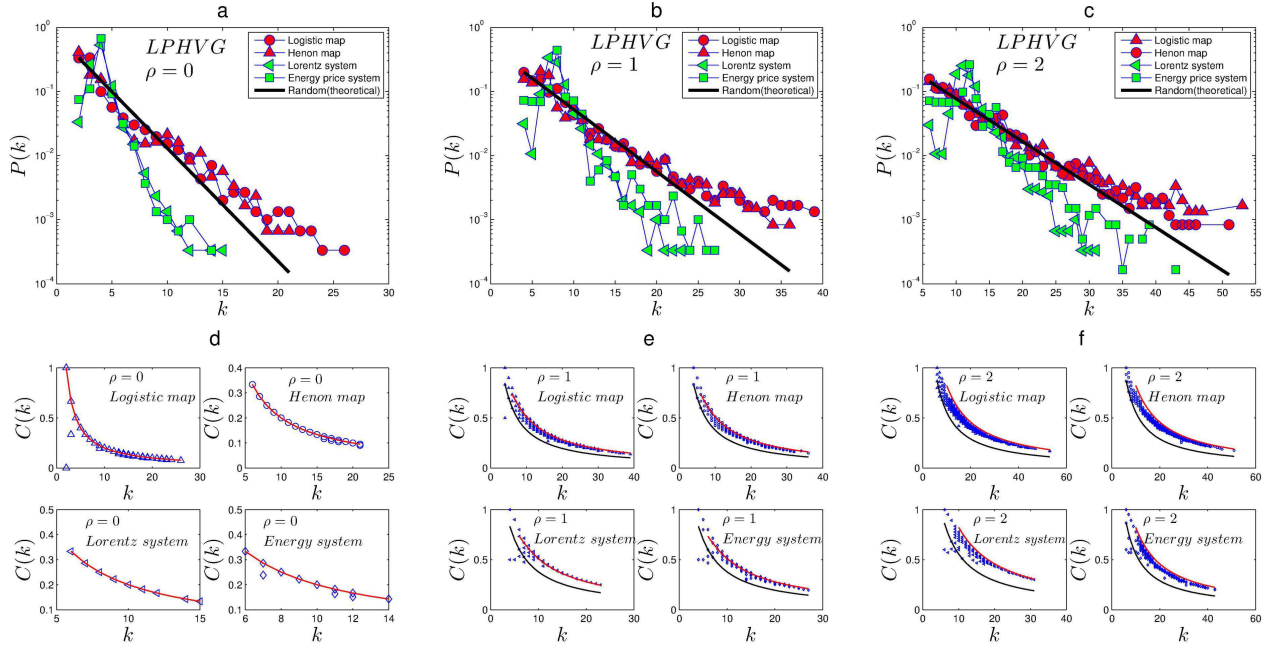


FIG. 6: The upper part: Semilog plot of the degree distributions of Limited penetrable horizontal visibility graphs associated to series generated through Logistic map, Henon map, Lorenz chaotic system and Energy price- supply-economic growth system. The bottom part: The relationship between degree and clustering coefficients.

**Application to real crude oil future price series.** As a further example, we use data from the U.S. Energy Information Administration on the crude oil future contract 1 (Dollars per Barrel) from 4 April 1983 to 28 March 1985, and find that they

exhibit chaotic and long-range correlations [38–39]. We select 500 sample data points and demonstrate that we can use our method to distinguish chaotic series from random series when the data sample is small (although for theoretical results we need infinite data). Fig. 7 shows the results of the horizontal visibility graph [see Fig. 7(a)] and the limited penetrable horizontal visibility graph [see Fig. 7(b)] of 500 data points extracted from crude oil futures. We find that the degree distributions both deviate from Eq. (2), which means the crude oil future price sequence is not random but chaotic. Comparing the results of HVG ( $\rho = 0$  in LPHVG) and LPHVG, we find that here LPHVG works better than HVG because the selected crude oil price series is too short and there are fewer links in HVG. An advantage in this case is that we can choose a suitable parameter  $\rho$  when constructing LPHVG.

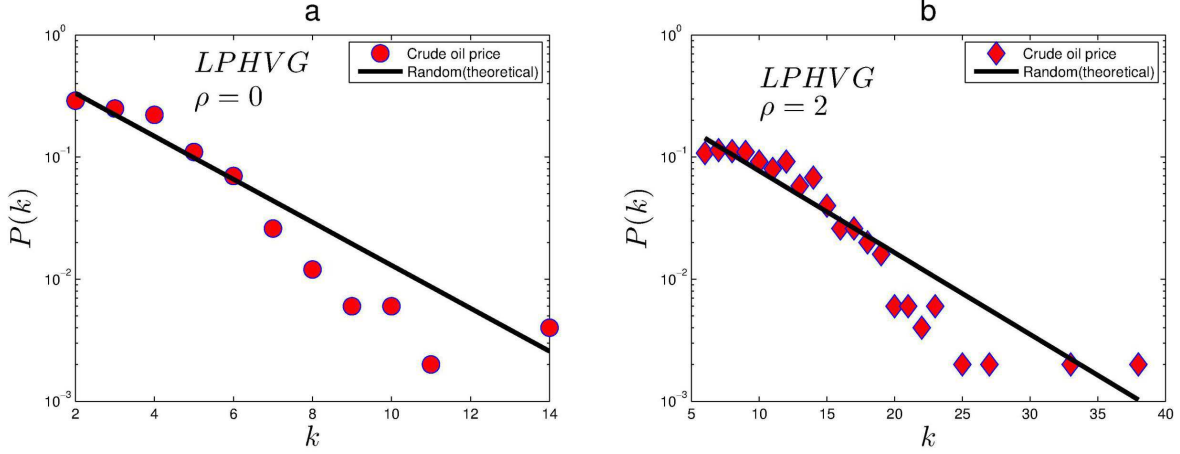


FIG. 7: Semilog plot of the degree distributions of LPHVGs associated to crude oil price series.

To further illustrate the application, we draw on the above analysis and use LPVHG ( $\rho = 2$ ) to describe the global evolution of crude oil future prices (for the calculation process see Methods). Our sample data is from the crude oil future contract 1 (in dollars per barrel) from 4 April 1983 to 15 August 2017 [see Fig. 8(a)]. Because fluctuations in crude oil future prices differ in different time periods, we separate our data into two periods, a more stable period from 4 April 1983 to 10 February 2004 and a period of sharp fluctuations from 11 February 2004 to 15 August 2017 [19]. Using our calculation method (see the Method section) we establish eighty-two 100-week time series windows (i.e.,  $L = 500$ ), the first of which is from 4 April 1983 to 28 March 1985. Because each window moves 20 weeks to generate the next window (i.e.,  $l = 100$ ), two adjacent windows have overlaps of 80 weeks. This enables information from one window to move to the next in succession. Each window contributes 500 nodes to building the local limited penetrable visibility graph network. Figs 8(b) and 8(c) show the evolution of the adjacency matrix of LPHVGs associated with a random series extracted from a uniform distribution and from crude oil price series, respectively. Note that adjacent matrices in the random time series and the crude oil price time series significantly differ, but their respective adjacent matrices in different time windows are similar. Figures 8(d)–8(f) show the evolution of the mean degree, mean clustering coefficient and mean path length, respectively. We find that the mean degree, mean clustering coefficient and mean path length of the LPHVG associated with the random series agree with the theoretical values, but these three quantities of LPHVG associated with the crude oil price series do not. The levels of mean degree of the LPHVG associated with the crude oil price series are smaller than the theoretical values, but the mean clustering coefficient and mean path length are larger. They also show different trends in different fluctuation periods. Values in the sharp fluctuation period are larger than

values in the stable fluctuation period. Figs 8(g)–(i) show the global evolution of random series and crude oil price series (see Eqs (12)–(16) in Methods). Note that the random time series has neither short-range nor long-range correlations, but the crude oil price time series has both. Thus using LPHVG enables us to describe the global time series evolution.

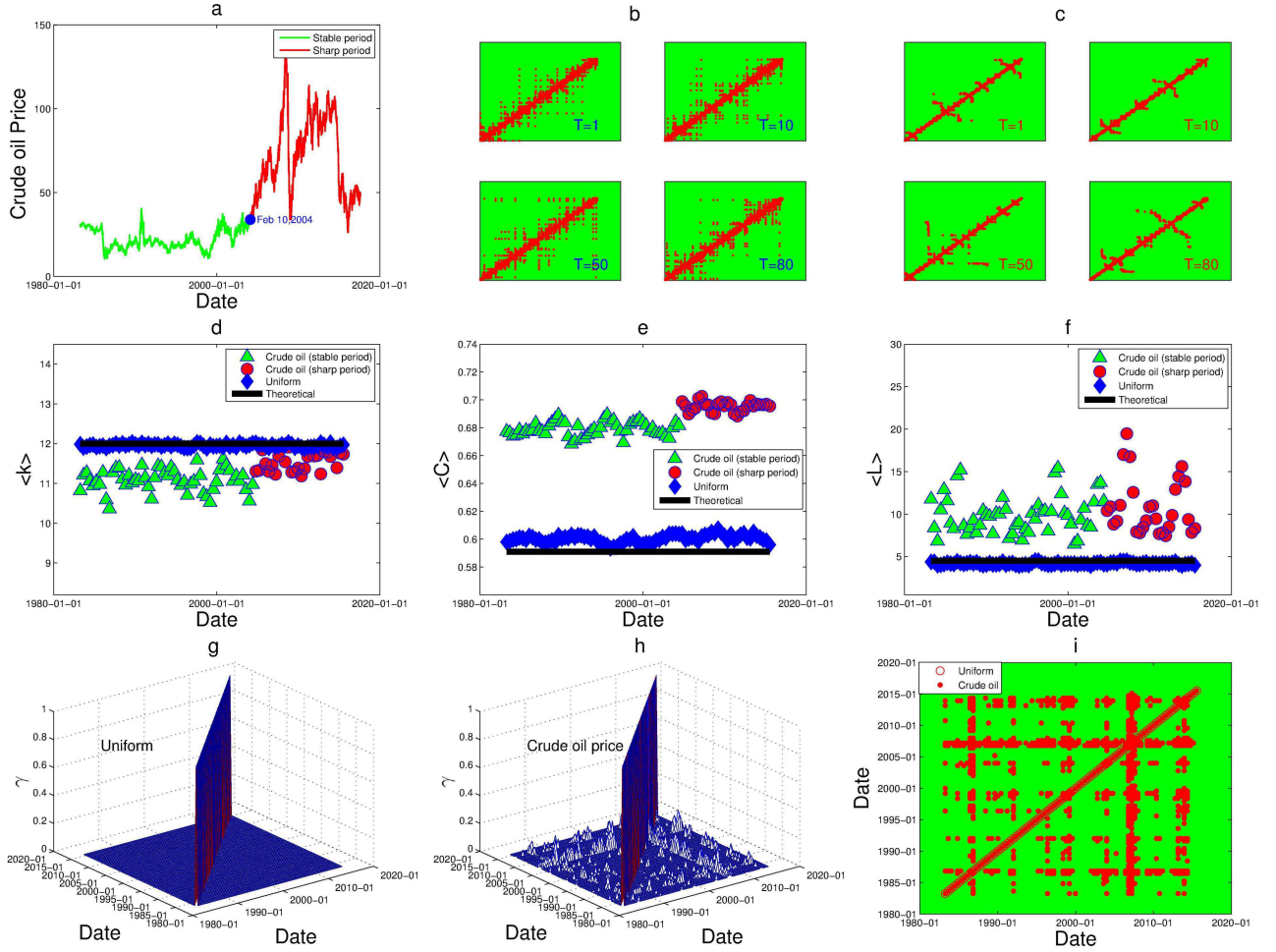


FIG. 8: (a) Crude oil price series, the green line represents the stable period and the red line represents the sharp period. (b) Evolution of the adjacency matrix of LPHVGs associated to the random series extracted from a uniform distribution. (c) Evolution of the adjacency matrix of LPHVGs associated to crude oil price series. (d) Evolution of the mean degree of the LPHVGs associated to random series, crude oil price series and the theoretical value. (e) Evolution of the mean clustering coefficient of the LPHVGs associated to random series, crude oil price series and the theoretical value. (f) Evolution of the mean path length of the LPHVGs associated to random series, crude oil price series and the theoretical value. (g) The correlation index distribution of random series. (h) The correlation index distribution of crude oil price series. (i) The recursive graph of correlation index associated to random series and crude oil price series.

### III. DISCUSSION

We have introduced a limited penetrable horizontal visibility algorithm, a more generalized case of the horizontal visibility algorithm [11–12] in which the limited penetrable distance is  $\rho = 0$ . We obtain exact results on several properties of the limited penetrable horizontal visibility graph associated with a general uncorrelated random series, the reliability of which has been confirmed by numerical simulations. In particular, the degree distribution of the graph has the exponential form  $P(k) \sim \exp[-\lambda(k - 2\rho - 2)]$ ,  $\lambda = \ln[(2\rho + 3)/(2\rho + 2)]$ ,  $\rho = 0, 1, 2, \dots, k = 2\rho + 2, 2\rho + 3, \dots$ . The calculated expression of mean degree  $\langle k \rangle = 4(\rho + 1)(1 - \frac{2\rho + 1}{2T})$  holds for every periodic or aperiodic series  $T \rightarrow \infty$ , independent of the deterministic process that generates them. The clustering coefficient  $C$  has a relationship with degree  $k$ , i.e.,  $C_{\min}(k) = \frac{2}{k} + \frac{2\rho(k-2)}{k(k-1)}$ ,  $\rho = 0, 1, 2, k \geq 2(\rho + 1)$ ,  $C_{\max}(k) = \frac{2}{k} + \frac{4\rho(k-3)}{k(k-1)}$ ,  $\rho = 0, 1, 2, k \geq 2(2\rho + 1)$ . The probability  $P_\rho(n) = \frac{2\rho(\rho+1)+2}{n(n+1)}$  introduces shortcuts to the limited penetrable horizontal visibility graph that exhibit a small-world phenomenon. Because these results are independent of the distribution from which the series was generated, we conclude that all uncorrelated random series have the same limited penetrable horizontal visibility graph and, in particular, the same degree distribution, mean degree, clustering coefficient distribution, and small world characteristics. This algorithm can thus be used as a simple test for discriminating uncorrelated randomness from chaos. We show that the method can distinguish between random series that follow the theoretical predictions and chaotic series that deviate from them. In addition, we employ the method to measure the global evolution characteristics of time series by using LPHVG, and the empirical results confirm its validity.

Our exact results presented here are extension of previous work [11]. We adjust the limited penetrable parameter  $\rho$  to the actual situation in order to distinguish chaos from uncorrelated randomness. The method can serve as a preliminary test for locating deterministic fingerprints in time series. If we determine that  $P(k)$  has an exponential tail that deviates from Eq. (2), or that  $C(k)$  deviates from Eqs. (6) and (7), we apply embedding methods to the series. Topics of further research could include whether this algorithm is also able to quantify chaos, the relationship between such standard chaos indicators as Lyapunov exponents and the correlation dimension, how to tune the limited penetrable parameter  $\rho$ , how to use the limited penetrable horizontal visibility graph to handle two-dimensional manifolds, the topological properties of the visibility graphs (VG) and limited penetrable visibility graphs (LPVG), and expanded applications of LPHVG.

### IV. METHODS

**Limited Penetrable Horizontal Visibility Graph (LPHVG).** The limited penetrable visibility graph (LPVG) [30] and the multiscale limited penetrable horizontal visibility graph (MLPHVG) [14] are a recent extension of the VG [9] and HVG [11–12] used to analyze nonlinear time series. The limited penetrable horizontal visibility graph (LPHVG) is a geometrically more simple and analytically solvable version of LPVG [30] and MLPHVG [14]. To define it we let  $\{x_i\}_{i=1,2,\dots,N}$  be a time series of  $N$  real numbers. If we set the limited penetrable distance to  $\rho$ , LPHVG maps the time series into a graph with  $N$  nodes and an adjacency matrix  $\mathbf{A}$ . Nodes  $i$  and  $j$  are connected through an undirected edge ( $A_{ij} = A_{ji} = 1$ ) when  $x_i$  and  $x_j$  have limited penetrable horizontal visibility (see Fig. 9), i.e., if at most  $\rho$  intermediate data  $x_q$  is

$$x_q \geq \inf\{x_i, x_j\}, \forall q \in (i, j). \quad (11)$$

This mapping is a limited penetrable horizontal visibility graph (LPHVG). When we set the limited penetrable distance  $\rho = 0$ , LPHVG degenerates into HVG [11]. When  $\rho \neq 0$ , there are more connections between any two nodes in LPHVG than in HVG.

Fig. 9(b) shows the new established connections (red lines) when we infer the LPHVG on the basis of HVG with a limited penetrable distance  $\rho = 1$ . Note that the limited penetrable horizontal visibility graph of a given time series has all the properties of its horizontal visibility graph, e.g., it is connected and invariant under all affine transformations of the series data [9, 11].

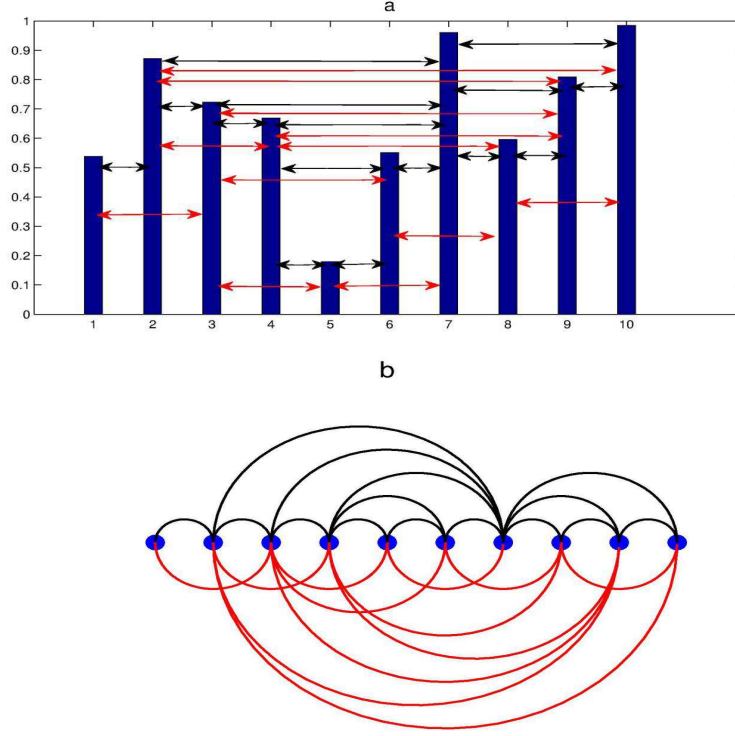


FIG. 9: Example of (a) a time series (10 data values) and (b) its corresponding LPHVG with the limited penetrable distance  $\rho$  being 1, where every node corresponds to time series data in the same order. The limited penetrable horizontal visibility lines between data points define the links connecting nodes in the graph.

**Measurement of the Global Evolution Characteristics of Time Series using LPHVG.** A time series is defined  $\mathbf{X} = \{x(t)\}, t = 1, 2, \dots, N$ . To characterize the evolution of the time series using LPHVG, we divide the time series of the entire scale of the time window into equal small-scale segments and assume that the length of the sliding window is  $L$ . We define  $l$  the step length between sliding time windows. To ensure that small-scale segments of the time series are continuous, we require that  $l < L$ . This allows us to obtain  $T = \lfloor (N - L)/l + 1 \rfloor$  small-scale time windows, where  $\lfloor \dots \rfloor$  is the rounding function. For every small-scale time window  $t$ , we transform time series into the  $LPHVG(t)$  using the limited penetrable horizontal visibility algorithm. The topological structure of LPHVG changes with time  $t$ . To describe this process from the global perspective, we use the Euclidean distance to measure the relationship between LPHVGs. We define the Euclidean distance between  $LPHVG(t_m)$  and  $LPHVG(t_n)$  to be

$$d(LPHVG(t_m), LPHVG(t_n)) = \sqrt{\sum_{i=1}^L \sum_{j=1}^L (a_{ij}^{(t_m)} - a_{ij}^{(t_n)})^2}, a_{ij}^{(t_m)} \in \mathbf{A}^{t_m}, a_{ij}^{(t_n)} \in \mathbf{A}^{t_n}. \quad (12)$$

We then determine the distance matrix

$$\mathbf{D}_{T \times T} = \{d_{t_m, t_n}\}_{t_m=1,2,\dots,T, t_n=1,2,\dots,T}, \quad (13)$$

and assign a threshold value to  $\theta$

$$\theta = \min\{d_{t_m, t_n}^{\text{rand}}\}_{t_m \neq t_n}, d_{t_m, t_n}^{\text{rand}} \in \mathbf{D}_{T \times T}^{\text{rand}}. \quad (14)$$

Here  $\mathbf{D}_{T \times T}^{\text{rand}}$  is the distance matrix associated with the independent and identically distributed random time series. Using the threshold  $\theta$ , we define the correlation index  $\gamma$ ,

$$\gamma_{t_m, t_n} = \begin{cases} 0, & d_{t_m, t_n} \geq \theta. \\ 1 - d_{t_m, t_n} / \theta, & d_{t_m, t_n} < \theta. \end{cases} \quad (15)$$

Here  $\gamma_{t_m, t_n}$  is the correlation degree of LPHVG at time  $t_m$  and time  $t_n$ , and  $\gamma_{t_m, t_n}$  can be visualized using a recursive graph constructed using the formula

$$\mathfrak{R}(t_m, t_n) = \Theta(\theta - d(LPHVG(t_m), LPHVG(t_n))), \Theta(x) = \begin{cases} 1, & x > 0, \\ 0, & x \leq 0, \end{cases} \quad (16)$$

where  $\Theta(x)$  is the Heaviside function. We use the formula to plot the relationship between LPHVGs in two-dimensional coordinates in which both the abscissa and the ordinate are at time  $t$ . In the recursive graph when the Euclidean distance between  $LPHVG(t_m)$  and  $LPHVG(t_n)$  is sufficiently close, i.e., when  $\mathfrak{R}(t_m, t_n) = 1$ , we plot the red dot at  $(t_m, t_n)$  and  $(t_n, t_m)$ . Note that at  $(t_m, t_m)$  and  $(t_n, t_n)$ , i.e., at the main diagonal, the red dots remain throughout, and we can use it to characterize the global dynamic changes in correlation.

## V. ACKNOWLEDGMENTS

The Research was supported by the following foundations: The National Natural Science Foundation of China (71503132, 71690242, 91546118, 11731014, 71403105, 61403171), Qing Lan Project of Jiangsu Province (2017), University Natural Science Foundation of Jiangsu Province (14KJA110001), Jiangsu Center for Collaborative Innovation in Geographical Information Resource Development and Application, CNPq, CAPES, FACEPE and UPE.

## VI. APPENDIX

**Theorem S1.** Let  $X(t)$  be a real bi-infinite time series of *i.i.d.* random variables with probability density  $f(x)$ , with  $x \in [a, b]$ , and consider its associated LPHVG with a limited penetrable distance  $\rho = 1$ . Then

$$P(k) \sim \exp[-(k-4)\ln(5/4)], k = 4, 5, \dots, \forall f(x).$$

**Proof:** Using a method similar to that presented in Refs. [10,11], we select a generic datum  $x_0$  to be the seed. We calculate the probability that an arbitrary datum with value  $x_0$  has a limited penetrable visibility of exactly  $k$  other data. From the definition of LPHVG, when  $x_0$  has penetrable visibility of  $k$  data there will be at least two penetrable data and two bounding data, one

penetrable and one bounding datum on the right-hand side of  $x_0$  and one on the left-hand side, such that the  $k - 4$  remaining visible and penetrable visible data are located inside two bounding data. Note that  $k = 4$  is the minimum possible degree (see Fig. S1).

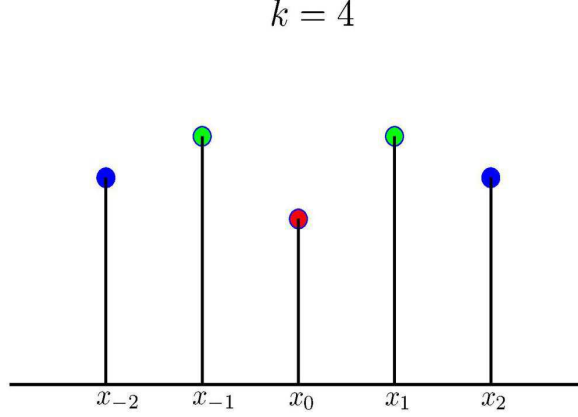


**Fig.S1.** Set of possible configuration for a seed data  $x_0$  with  $k = 4$ . The green dots are penetrable data, the blue dots are bounding data.

To derive the degree distribution of the associated LPHVG, we first compute some easy terms. Fig. S1 shows the simplest case  $P(k = 4)$  in which there are two penetrable data ( $x_{-1}, x_1$ ) and two bounding data ( $x_{-2}, x_2$ ). To assure that  $k = 4$ , we set the height of both the penetrable and bounding data greater than  $x_0$ , i.e.,  $x_{-1} \geq x_0, x_1 \geq x_0$  and  $x_{-2} \geq x_0, x_2 \geq x_0$ . Then

$$P(k = 4) = Prob(x_{-2}, x_{-1}, x_1, x_2 \geq x_0) \quad (S1)$$

$$= \int_a^b f(x_0)dx_0 \int_{x_0}^b f(x_{-2})dx_{-2} \int_{x_0}^b f(x_{-1})dx_{-1} \int_{x_0}^b f(x_1)dx_1 \int_{x_0}^b f(x_2)dx_2.$$

In order to simplify Eq. (S1), we define the cumulative probability distribution function  $F(x)$  of any probability density  $f(x)$  to be

$$F(x) = \int_a^x f(t)dt, \quad (S2)$$

where  $dF(x)dx = f(x), F(a) = 0$  and  $F(b) = 1$ . With a loss of generality, we assume  $a = 0, b = 1$ , i.e.,  $F(0) = 0$  and  $F(1) = 1$ . Here the relation between  $f$  and  $F$  holds, i.e.,

$$\frac{dF^{(n)}(x)}{dx} = n f(x) F^{n-1}(x). \quad (S3)$$

Using Eqs. (S2) and (S3), we rewrite Eq. (S1) to be

$$P(k = 4) = \int_0^1 f(x_0)[1 - F(x_0)]^4 dx_0 = \frac{1}{5}, \forall f(x). \quad (S4)$$

When  $P(k = 5)$  (see Fig. S2), four configurations emerge: Case 1:  $C_0^1$ , in which  $x_0$  has penetrable variables  $x_{-1}$  and  $x_1$ , bounding variables  $x_{-2}$  and  $x_3$ , and a right-hand side inner variable  $x_2$ . Case 2:  $C_0^2$ , in which  $x_0$  has penetrable variables  $x_{-1}$  and  $x_2$ , bounding variables  $x_{-2}$  and  $x_3$ , and a right-hand side inner variable  $x_1$ . Case 3:  $C_1^1$ , in which  $x_0$  has penetrable variables

$x_{-2}$  and  $x_1$ , bounding variables  $x_{-3}$  and  $x_2$ , and a left-hand side inner variable  $x_{-1}$ . Case 4:  $C_1^2$ , in which  $x_0$  has penetrable variables  $x_{-1}$  and  $x_1$ , bounding variables  $x_{-3}$  and  $x_2$ , and a left-hand side inner variable  $x_{-2}$ .

Thus

$$P(k=5) = P(C_0^1) + P(C_0^2) + P(C_1^1) + P(C_1^2) \equiv p_0^1 + p_0^2 + p_1^1 + p_1^2. \quad (S5)$$

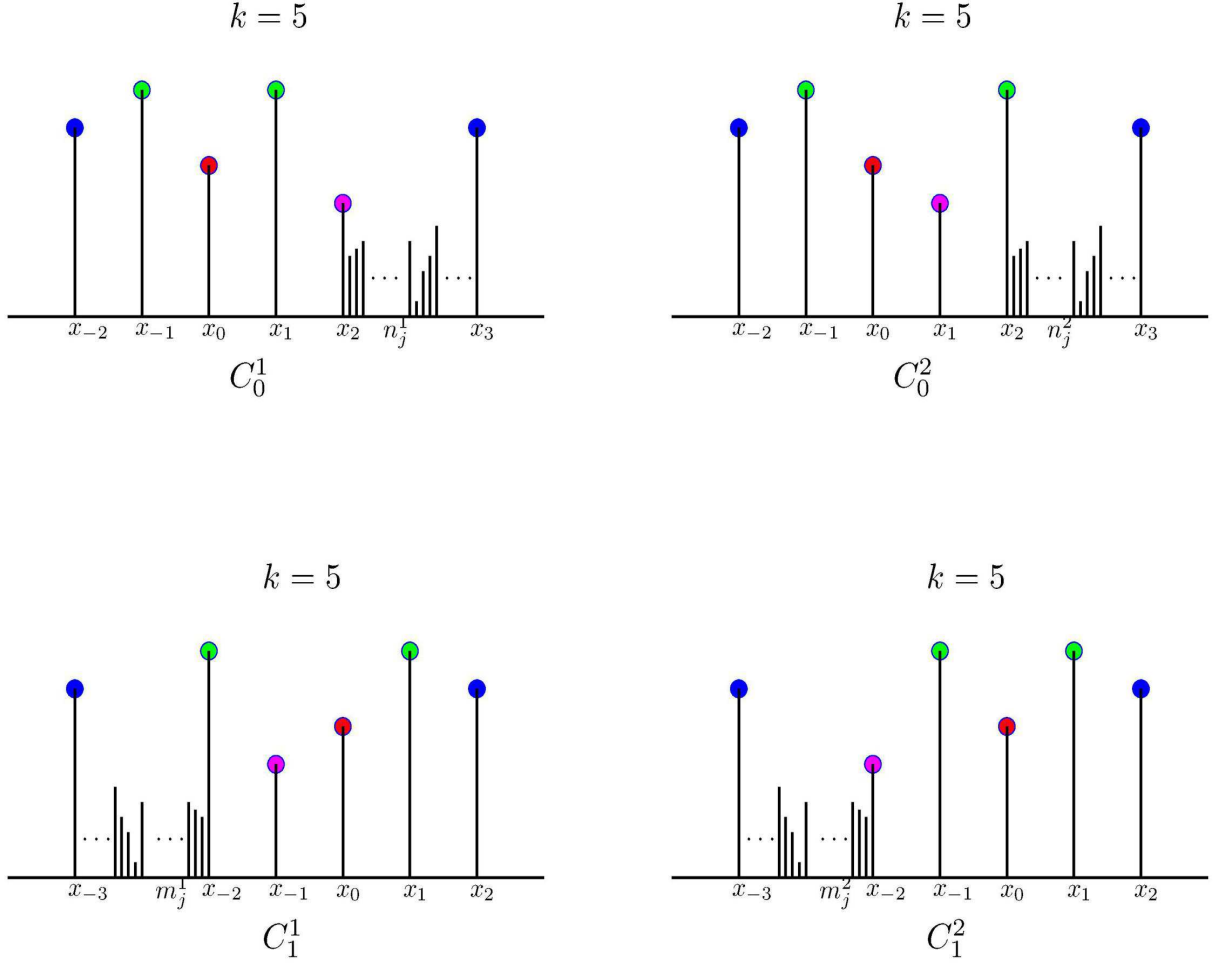


**Fig.S2.** Set of possible configurations for a seed data  $x_0$  with  $k=5$ . The sign of the subscript in  $x_i$  indicates whether the data are located on the left-hand side of  $x_0$  or on the right-hand side. The sign of the subscript in  $C_i^j$  indicates the number of inner data located on the left-hand side of  $x_0$ , the superscript in  $C_i^j$  indicates the different cases. The signs  $n_j^1, n_j^2, m_j^1, m_j^2$  indicate the number of the hidden data.

Note that an arbitrary number of hidden variables  $n_j^1, n_j^2, m_j^1, m_j^2$  eventually are located between the inner data and the bounding variables (or the penetrable data and the bounding data) and this must be taken into account in the probability calculation. The geometrical restrictions for the hidden variables are  $n_j^1 < x_2, n_j^2 < x_1, j = 1, 2, \dots, r$  for  $C_0^1, C_0^2$  and



$m_j^1 < x_{-1}, m_j^2 < x_{-2}, j = 1, 2, \dots, s$  for  $C_1^1, C_1^2$ . Then

$$\begin{aligned} p_0^1 &= \text{Prob}((x_{-2}, x_{-1}, x_1, x_3 \geq x_0) \cap (x_2 < x_0) \cap (\{n_j^1 < x_2\}_{j=1,2,\dots,r})), \\ p_0^2 &= \text{Prob}((x_{-2}, x_{-1}, x_2, x_3 \geq x_0) \cap (x_1 < x_0) \cap (\{n_j^2 < x_1\}_{j=1,2,\dots,r})), \\ p_1^1 &= \text{Prob}((x_{-3}, x_{-2}, x_1, x_2 \geq x_0) \cap (x_{-1} < x_0) \cap (\{m_j^1 < x_{-1}\}_{j=1,2,\dots,s})), \\ p_1^2 &= \text{Prob}((x_{-3}, x_{-1}, x_1, x_2 \geq x_0) \cap (x_{-2} < x_0) \cap (\{m_j^2 < x_{-2}\}_{j=1,2,\dots,s})). \end{aligned} \quad (S6)$$

Because these are independent and identically distributed random variables,  $p_0^1$  can be calculated

$$\begin{aligned} p_0^1 &= \int_0^1 f(x_0)dx_0 \int_{x_0}^1 f(x_{-2})dx_{-2} \int_{x_0}^1 f(x_{-1})dx_{-1} \int_{x_0}^1 f(x_1)dx_1 \int_{x_0}^1 f(x_3)dx_3 \int_0^{x_0} f(x_2)dx_2 \\ &+ \sum_{r=1}^{\infty} \int_0^1 f(x_0)dx_0 \int_{x_0}^1 f(x_{-2})dx_{-2} \int_{x_0}^1 f(x_{-1})dx_{-1} \int_{x_0}^1 f(x_1)dx_1 \int_{x_0}^1 f(x_3)dx_3 \int_0^{x_0} f(x_2)dx_2 \prod_{j=1}^r \int_0^{x_2} f(n_j^1)dn_j^1. \end{aligned} \quad (S7)$$

From Eq. (S3) we now have

$$\begin{aligned} p_0^1 &= \int_0^1 f(x_0)dx_0 \int_{x_0}^1 f(x_{-2})dx_{-2} \int_{x_0}^1 f(x_{-1})dx_{-1} \int_{x_0}^1 f(x_1)dx_1 \int_{x_0}^1 f(x_3)dx_3 \int_0^{x_0} \frac{f(x_2)}{1-F(x_2)}dx_2 \\ &= -\int_0^1 f(x_0)dx_0 [1-F(x_0)]^4 \ln[1-F(x_0)] = \frac{1}{25}. \end{aligned} \quad (S8)$$

Using the same method, we find the identical results for  $p_0^2, p_1^1$  and  $p_1^2$  and then we have

$$P(k=5) = 4P_0^1 = -4 \int_0^1 f(x_0)dx_0 [1-F(x_0)]^4 \ln[1-F(x_0)] = \frac{4}{25}. \quad (S9)$$

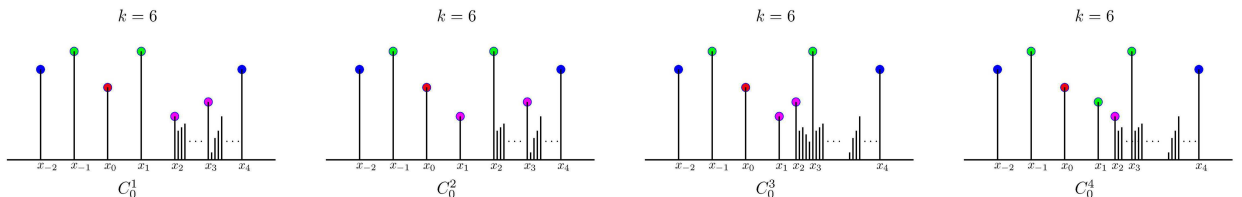
We thus conclude that a configuration  $C_i^j$  contributes to  $P(k)$  with a product of internals when (i) the seed variable  $[S]$  provides a contribution of  $\int_0^1 f(x_0)dx_0$ , (ii) each penetrable variable  $[P]$  provides a contribution of  $\int_{x_0}^1 f(x)dx$ , (iii) each boundary variable  $[B]$  provides a contribution of  $\int_{x_0}^1 f(x)dx$ , and (iv) an inner variable  $[I]$  provides a contribution of  $\int_{x_j}^{x_0} \frac{f(x)}{1-F(x)}$ .

Using these four rules, we formally schematize the probability associated with each configuration. For example, when  $k=4$ ,  $P(k)$  has a single contribution  $p_0$  shown in the formal diagram  $[B][P][S][P][B]$ . When  $k=5$ ,  $P(k) = p_0^1 + p_0^2 + p_1^1 + p_1^2$  where  $p_0^1$  is shown in the diagram  $[B][P][S][P][I][B]$ ,  $p_0^2$  is shown in  $[B][P][S][I][P][B]$ ,  $p_1^1$  is shown in  $[B][P][I][S][P][B]$ , and  $p_1^2$  is shown in  $[B][I][P][S][P][B]$ . Thus we derive a general expression for  $P(k)$  by applying the four rules for the contribution of each  $C_i^j, i=0, 1, 2, \dots, j=1, 2, \dots$ . When  $k=6$ , however, there are 13 possible seed data  $x_0$  configurations, and it is labeled  $C_0^i, C_1^j, C_2^r$ .

Similar to  $P(k=5)$ , we derive

$$P(k=6) = \sum_{i=1} p_0^i + \sum_{j=1} p_1^j + \sum_{r=1} p_2^r. \quad (S10)$$

Here  $C_1^j$  leads to the same expression as configurations in  $k=5$  and thus we can derive  $p_1^j$  by applying the four rules. Fig. S3 shows that  $C_0^i$  and  $C_2^r$  are geometrically different and are formed from a seed  $x_0$  and two penetrable variables. In configurations  $C_0^4$  and  $C_2^4$  there are three penetrable variables, one of which ( $x_1$  in  $C_0^4$  and  $x_{-1}$  in  $C_2^4$ ) is smaller than  $x_0$ . When calculating  $P(k)$  the role of this smaller penetrable variable is similar to the inner variable. Thus without loss of generality we refer to this smaller penetrable variable as the inner variable. There are two bounding and two concatenated inner variables, and the concatenated variables produce concatenated integrals.



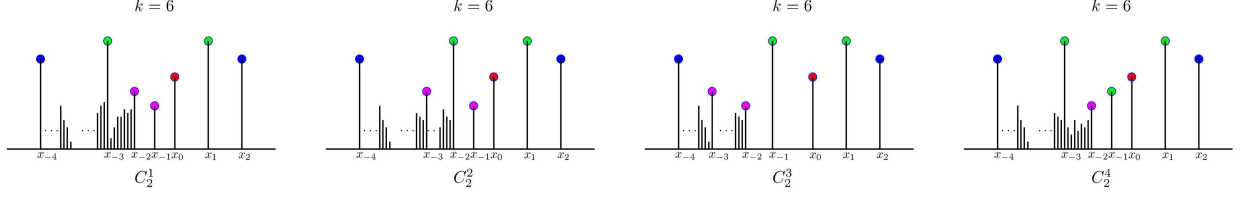


**Fig.S3.** Set of possible configurations for  $C_0^i, C_2^r$  with  $k = 6$ .

For example, when we apply the same formalism as for  $k = 5$  we find that when  $k = 6$ , in the case of  $C_0^i$ ,

$$\begin{aligned}
 p_0^1 &= \int_0^1 f(x_0)dx_0 \int_{x_0}^1 f(x_1)dx_1 \int_0^{x_0} \frac{f(x_2)}{1-F(x_2)}dx_2 \int_{x_2}^{x_0} \frac{f(x_3)}{1-F(x_3)}dx_3 \int_{x_0}^1 f(x_4)dx_4 \int_{x_0}^1 f(x_{-1})dx_{-1} \int_{x_0}^1 f(x_{-2})dx_{-2} \\
 p_0^2 &= \int_0^1 f(x_0)dx_0 \int_0^{x_0} \frac{f(x_1)}{1-F(x_1)}dx_1 \int_{x_0}^1 f(x_2)dx_2 \int_{x_1}^{x_0} \frac{f(x_3)}{1-F(x_3)}dx_3 \int_{x_0}^1 f(x_4)dx_4 \int_{x_0}^1 f(x_{-1})dx_{-1} \int_{x_0}^1 f(x_{-2})dx_{-2} \\
 p_0^3 &= \int_0^1 f(x_0)dx_0 \int_0^{x_0} \frac{f(x_1)}{1-F(x_1)}dx_1 \int_{x_1}^{x_0} \frac{f(x_2)}{1-F(x_2)}dx_2 \int_{x_0}^1 f(x_3)dx_3 \int_{x_0}^1 f(x_4)dx_4 \int_{x_0}^1 f(x_{-1})dx_{-1} \int_{x_0}^1 f(x_{-2})dx_{-2} \\
 p_0^4 &= \int_0^1 f(x_0)dx_0 \int_0^{x_0} \frac{f(x_1)}{1-F(x_1)}dx_1 \int_0^{x_1} f(x_2)dx_2 \int_{x_0}^1 f(x_3)dx_3 \int_{x_0}^1 f(x_4)dx_4 \int_{x_0}^1 f(x_{-1})dx_{-1} \int_{x_0}^1 f(x_{-2})dx_{-2}
 \end{aligned} \tag{S11}$$

Using Eq. (S8), when  $k = 5$ , every integral depends on  $x_0$ , and thus we integrate each term to find this dependence on. Here, however, there are two concatenated inner variables, and two concatenated inner variables generate the dependence on the integrals and hence on the probabilities. Thus in the general case each configuration is not equiprobable and does not provide the same contribution to the probability  $P(k)$ . To weight the effect of these concatenated contributions, we use the definition of  $p_i$ . Since  $P(k)$  is formed by  $k - 3$  contributions labeled  $C_0^i, C_1^j, \dots, C_{k-4}^r$  in which the subindex denotes the number of inner data present at the left-hand side of seed  $x_0$ , we conclude that in general the  $k - 4$  inner variables make the following contributions to  $P(k)$ :

- (a)  $p_0^i$  has  $k - 4$  concatenated internals (the right-hand side of seed  $x_0$ );
- (b)  $p_1^j$  has  $k - 5$  concatenated internals (the right-hand side of seed  $x_0$ ) and an independent inner data contribution (the left-hand side of seed  $x_0$ );
- (c)  $p_2^r$  has  $k - 6$  concatenated internals (the right-hand side of the seed  $x_0$ ) and another two independent inner data contributions (the left-hand side of seed  $x_0$ );
- ⋮
- (d)  $p_{k-5}^j$  has  $k - 5$  concatenated internals (the left-hand side of seed  $x_0$ ) and an independent inner data contribution (the right-hand side of seed  $x_0$ ); and
- (e)  $p_{k-4}^i$  has  $k - 4$  concatenated internals (the left-hand side of seed  $x_0$ ).

Note that  $p_m^n$  is symmetric with respect to the seed and the penetrable variables. Adding this modification to the four rules we calculate a general expression for  $P(k)$ , i.e.,

$$\begin{aligned}
 P(k) &= \sum_i p_0^i + \sum_j p_1^j + \sum_r p_2^r + \dots + \sum_j p_{k-5}^j + \sum_i p_{k-4}^i \\
 &= \sum_i [S][P]^2[B]^2[I]_0^i[I]_{k-4}^i + \sum_j [S][P]^2[B]^2[I]_1^j[I]_{k-5}^j + \sum_r [S][P]^2[B]^2[I]_2^r[I]_{k-6}^r + \dots \\
 &\dots + \sum_j [S][P]^2[B]^2[I]_{k-5}^j[I]_1^j + \sum_i [S][P]^2[B]^2[I]_{k-4}^i[I]_0^i.
 \end{aligned} \tag{S12}$$

Using mathematical induction, we prove that

$$P(k) = \sum_{h=0}^{k-4} 3^h [S][P]^2 [B]^2 [I]_h [I]_{k-4-h}, \quad (S13)$$

where the concatenation of  $h$  inner variable integrals  $[I]_h$  is

$$[I]_h = \int_0^{x_0} \frac{f(x_1)}{1-F(x_1)} dx_1 \prod_{j=1}^{h-1} \int_{x_j}^{x_0} \frac{f(x_{j+1})}{1-F(x_{j+1})} dx_{j+1} = \frac{(-1)^h}{h!} [\ln(1-F(x_0))]^h. \quad (S14)$$

Using Eq. (S13) and Eq. (S14), we have

$$\begin{aligned} P(k) &= \sum_{h=0}^{k-4} 3^h \frac{(-1)^{k-4}}{h!(k-4-h)!} \int_0^1 f(x_0) [1-F(x_0)]^4 [\ln(1-F(x_0))]^{k-4} dx_0 \\ &= \left(\frac{1}{5}\right)^{k-3} \sum_{h=0}^{k-4} \frac{3^h (k-4)!}{h!(k-4-h)!} = \frac{1}{5} \left(\frac{4}{5}\right)^{k-4}, \forall f(x). \end{aligned} \quad (S15)$$

Note that  $P(k)$  can be rewritten

$$P(k) \sim \exp[-(k-4)\ln(5/4)], k = 4, 5, 6, \dots, \forall f(x). \quad (S16)$$

**Theorem S2.** Let  $X(t)$  be a real valued bi-infinite time series of *i.i.d.* random variables with a probability density  $f(x)$  and with  $x \in [a, b]$ , and consider its associated LPHVG at a limited penetrable distance  $\rho$ . Then

$$P(k) \sim \exp\{-(k-2\rho-2)\ln[(2\rho+3)/(2\rho+2)]\}, \rho = 0, 1, 2, 3, \dots, k = 2\rho+2, 2\rho+3, \dots, \forall f(x).$$

**Sketch of the proof.** The proof follows a similar path as for LPHVG with the limited penetrable distance  $\rho = 1$  (see *Theorem S1*). Instead of Eq. (S13) we now have

$$P(k) = \sum_{h=0}^{k-2(\rho+1)} (2\rho+1)^h [S][P]^{2\rho} [B]^2 [I]_h [I]_{k-2(\rho+1)-h}. \quad (S17)$$

We prove by induction that

$$\begin{aligned} P(k) &= \sum_{h=0}^{k-2(\rho+1)} (2\rho+1)^h \frac{(-1)^{k-2(\rho+1)}}{h![k-2(\rho+1)-h]!} \int_0^1 f(x_0) [1-F(x_0)]^{2(\rho+1)} [\ln(1-F(x_0))]^{k-2(\rho+1)} dx_0 \\ &= \left(\frac{1}{2\rho+3}\right)^{k-2\rho-1} \sum_{h=0}^{k-2(\rho+1)} \frac{(2\rho+1)^h (k-2(\rho+1))!}{h![k-2(\rho+1)-h]!} = \frac{1}{2\rho+3} \left(\frac{2\rho+2}{2\rho+3}\right)^{k-2(\rho+1)}, \forall f(x), \end{aligned} \quad (S18)$$

i.e.,

$$P(k) \sim \exp\{-(k-2\rho-2)\ln[(2\rho+3)/(2\rho+2)]\}, \rho = 0, 1, 2, 3, \dots, k = 2\rho+2, 2\rho+3, \dots, \forall f(x). \quad (S19)$$

When  $\rho = 0$  using Eq. (S18) we find  $P(k) = \frac{1}{3} \left(\frac{2}{3}\right)^{k-2}$ , the result in Ref. [11]. When  $\rho = 0$  the LPHVG becomes the HVG. When  $\rho = 1$  the result is the same as in *Theorem S1*.

**Theorem S3.** Let  $X(t)$  be a real valued bi-infinite time series of *i.i.d.* random variable with probability density  $f(x)$  with  $x \in [a, b]$ , and consider its associated LPHVG with the limited penetrable distance  $\rho$ . Then the local clustering coefficient is

$$\begin{aligned} C_{\min}(k) &= \frac{2}{k} + \frac{2\rho(k-2)}{k(k-1)}, \rho = 0, 1, 2, k \geq 2(\rho+1), \\ C_{\max}(k) &= \frac{2}{k} + \frac{4\rho(k-3)}{k(k-1)}, \rho = 0, 1, 2, k \geq 2(2\rho+1). \end{aligned}$$

**Proof.** For a given node  $x_i$ , the local clustering coefficient  $C$  is the percentage of nodes connected to  $x_i$  that are connected to each other. Thus we calculate from a given node  $x_i$  the number of nodes from penetrable  $\rho$  visible to  $x_i$  have mutual penetrable  $\rho$  visibility (triangles), normalized with the set of possible triangles  $\binom{k}{2}$ .

In the simplest  $\rho = 1$  case, Fig. S1 shows that when a generic node  $x_i$  has a degree  $k = 4$  it has two penetrable data and two bounding data, and there are thus five triangles and  $C(k = 4) = 5/6$ . Fig. S2 shows that when a generic node  $x_i$  has a degree  $k = 5$  it has two penetrable data, two bounding data, and an inner datum. Here there are two possible outcomes. For configurations  $C_0^1, C_1^2$  there are seven triangles and  $C(k = 5) = 7/10$ . For configurations  $C_0^2, C_1^1$  there are eight triangles and  $C(k = 5) = 8/10$ . Fig. S3 shows that when a generic node  $x_i$  has a degree  $k = 6$  it has two penetrable data, two bounding data, and two inner data. Here there are three possible outcomes. For configuration  $C_1^3$  there are nine triangles and  $C(k = 6) = 9/15$ . For configurations  $C_0^1, C_0^2, C_1^1, C_1^2, C_1^4, C_2^2, C_2^3$  there are 10 triangles and  $C(k = 6) = 10/15$ . For configurations  $C_0^3, C_0^4, C_2^1, C_2^4$  there are 11 triangles and  $C(k = 6) = 11/15$ . Thus nodes having the same degree can have different clustering coefficients. Although the clustering coefficients of these nodes are irregular, the minimum clustering coefficient and the maximum clustering coefficient are regular.

The calculations of these minimum local clustering coefficients can be rewritten

$$\begin{aligned} C_{\min}(k = 4) &= [(k - 1) + (k - 2)\rho] / \binom{k}{2} = 5/6, \\ C_{\min}(k = 5) &= [(k - 1) + (k - 2)\rho] / \binom{k}{2} = 7/10, \\ C_{\min}(k = 6) &= [(k - 1) + (k - 2)\rho] / \binom{k}{2} = 3/5. \end{aligned} \quad (S20)$$

In general, for a degree  $k$  we can at a minimum form  $(k - 1) + (k - 2)\rho = (1 + \rho)k - (2\rho + 1)$  triangles out of  $\binom{k}{2}$  possibilities, and

$$C_{\min}(k) = [(1 + \rho)k - (2\rho + 1)] / \binom{k}{2} = \frac{2}{k} + \frac{2\rho(k-2)}{k(k-1)}, \rho = 0, 1, 2, k \geq 2(\rho + 1). \quad (S21)$$

Similarly, the calculation of the maximum local clustering coefficients can be rewritten

$$\begin{aligned} C_{\max}(k = 4) &= [(k - 1) + 2\rho(k - 3)] / \binom{k}{2} = 5/6, \\ C_{\max}(k = 5) &= [(k - 1) + 2\rho(k - 3)] / \binom{k}{2} = 8/10, \\ C_{\max}(k = 6) &= [(k - 1) + 2\rho(k - 3)] / \binom{k}{2} = 11/15. \end{aligned} \quad (S22)$$

For a degree  $k$  we can at a maximum form  $(k - 1) + 2\rho(k - 3) = (1 + 2\rho)k - (6\rho + 1)$  triangles out of  $\binom{k}{2}$  possibilities, and

$$C_{\max}(k) = [(1 + 2\rho)k - (6\rho + 1)] / \binom{k}{2} = \frac{2}{k} + \frac{4\rho(k-3)}{k(k-1)}, \rho = 0, 1, 2, k \geq 2(2\rho + 1). \quad (S23)$$

This relation between  $k$  and  $C_{\min}, C_{\max}$  allows us to deduce the local clustering coefficient distribution  $P(C_{\min})$  and  $P(C_{\max})$ ,

$$\begin{aligned} P(k) &= \frac{1}{2\rho+3} \left( \frac{2\rho+2}{2\rho+3} \right)^{k-2(\rho+1)}, \\ k &= \frac{\varphi + \sqrt{\varphi^2 - 8C_{\min}(2\rho+1)}}{2C_{\min}}, \varphi = C_{\min} + 2\rho + 2 \\ k &= \frac{\phi + \sqrt{\phi^2 - 8C_{\max}(6\rho+1)}}{2C_{\max}}, \phi = C_{\max} + 4\rho + 2. \end{aligned} \quad (S24)$$

Then

$$P(C_{\min}) = \frac{1}{2\rho+3} \exp\left\{ \left[ \frac{\varphi + \sqrt{\varphi^2 - 8C_{\min}(2\rho+1)}}{2C_{\min}} - 2(\rho + 1) \right] \ln\left( \frac{2\rho+2}{2\rho+3} \right) \right\}, \quad (S25)$$

$$P(C_{\max}) = \frac{1}{2\rho+3} \exp\left\{ \left[ \frac{\phi + \sqrt{\phi^2 - 8C_{\max}(6\rho+1)}}{2C_{\max}} - 2(\rho + 1) \right] \ln\left( \frac{2\rho+2}{2\rho+3} \right) \right\}. \quad (S26)$$

**Theorem S4.** Let  $\{x_t\}_{t=0,1,\dots,n}$  be a bi-finite sequence of *i.i.d.* random variables extracted from a continuous probability density  $f(x)$ . Then the probability  $P_\rho(n)$  that two data separated by  $n$  intermediate data are two connected nodes in the graph is

$$P_\rho(n) = \frac{2\rho(\rho + 1) + 2}{n(n + 1)}, \rho = 0, 1, 2, \dots$$

**Proof.** Without loss of generality, we restrict  $x$  to  $[0, 1]$ . When  $\rho = 0$ , Ref. [11] derives

$$P_0(n) = \int_0^1 \int_0^1 f(x_0)f(x_n)dx_0dx_n \int_0^{\min(x_0,x_n)} \dots \int_0^{\min(x_0,x_n)} f(x_1)\dots f(x_{n-1})dx_1\dots dx_{n-1} = \frac{2}{n(n+1)}. \quad (S27)$$

When  $\rho = 1$ , because an arbitrary value  $x_0$  from this series will be connected to node  $x_n$  if there is no more than one  $x_i \geq \min(x_0, x_n)$  for all  $x_i, i = 1, 2, \dots, n - 1$ . Then  $P_1(n)$  is

$$\begin{aligned} P_1(n) &= \int_0^1 \int_0^1 f(x_0)f(x_n)dx_0dx_n \int_0^{\min(x_0,x_n)} \dots \int_0^{\min(x_0,x_n)} f(x_1)\dots f(x_{n-1})dx_1\dots dx_{n-1} \\ &+ \int_0^1 \int_0^1 f(x_0)f(x_n) \int_{\min(x_0,x_n)}^1 f(x_1)dx_1 \int_0^{\min(x_0,x_n)} \dots \int_0^{\min(x_0,x_n)} f(x_2)\dots f(x_{n-1})dx_2\dots dx_{n-1} \\ &+ \dots + \int_0^1 \int_0^1 f(x_0)f(x_n) \int_{\min(x_0,x_n)}^1 f(x_{n-1})dx_{n-1} \int_0^{\min(x_0,x_n)} \dots \int_0^{\min(x_0,x_n)} f(x_1)\dots f(x_{n-2})dx_1\dots dx_{n-2}. \end{aligned} \quad (S28)$$

Since the integration limits are independent, when we rewrite  $x \equiv \min(x_0, x_n)$ , we have

$$\begin{aligned} P_1(n) &= \int_0^1 \int_0^1 f(x_0)f(x_n)F^{n-1}(x)dx_0dx_n + \binom{n-1}{1} \int_0^1 \int_0^1 f(x_0)f(x_n)[1 - F(x)]F^{n-2}(x)dx_0dx_n \\ &= \binom{n-1}{1} \int_0^1 \int_0^1 f(x_0)f(x_n)F^{n-2}(x)dx_0dx_n - (n-2) \int_0^1 \int_0^1 f(x_0)f(x_n)F^{n-1}(x)dx_0dx_n. \end{aligned} \quad (S29)$$

Without loss of generality we can fix  $x_0$  and move  $x_n$  such that the latter equation becomes

$$\begin{aligned} P_1(n) &= (n-1) \left[ \int_0^1 \int_0^{x_0} f(x_0)f(x_n)F^{n-2}(x_n)dx_0dx_n + \int_0^1 \int_{x_0}^1 f(x_0)f(x_n)F^{n-2}(x_0)dx_0dx_n \right] \\ &- (n-2) \left[ \int_0^1 \int_0^{x_0} f(x_0)f(x_n)F^{n-1}(x_n)dx_0dx_n + \int_0^1 \int_{x_0}^1 f(x_0)f(x_n)F^{n-1}(x_0)dx_0dx_n \right] \\ &= \frac{2}{n} - \frac{2(n-2)}{n(n+1)} = \frac{6}{n(n+1)}. \end{aligned} \quad (S30)$$

When  $P_\rho(n), \rho > 1$ , the calculation follows a path similar to that for  $P_1(n)$  such that instead of Eq. (S29) we have

$$P_\rho(n) = \int_0^1 \int_0^1 f(x_0)f(x_n)F^{n-1}(x)dx_0dx_n + \binom{n-1}{\rho} \int_0^1 \int_0^1 f(x_0)f(x_n)[1 - F(x)]^\rho F^{n-(\rho+1)}(x)dx_0dx_n. \quad (S31)$$

Then by induction we prove that

$$P_\rho(n) = \frac{2\rho(\rho+1)+2}{n(n+1)}, \rho = 0, 1, 2, \dots \quad (S32)$$

- 
- [1] Daw, C. S. et al. Self-Organization and Chaos in a Fluidized Bed. Phys. Rev. Lett. 75, 2308C2311 (1995).  
[2] Peng, C. K. et al. Mosaic organization of DNA nucleotides. Phys. Rev. E 49, 1685C1689 (1994).  
[3] Podobnik, B., Stanley, H. E. Detrended cross-correlation analysis: A new method for analyzing two nonstationary time series. Phys.Rev. Lett. 100, 084102 (2008).  
[4] Barabási A. L., Albert R. Emergence of scaling in random networks. science, 1999, 286(5439): 509-512.  
[5] Watts D. J., Strogatz S. H. Collective dynamics of small-worldnetworks. nature, 1998, 393(6684): 440-442.  
[6] Newman M. E. J., Watts D. J. Renormalization group analysis of the small-world network model. Physics Letters A, 1999, 263(4): 341-346.  
[7] Erdős P., Rényi A. On the existence of a factor of degree one of a connected random graph. Acta Mathematica Hungarica, 1966, 17(3-4): 359-368.  
[8] Zhang J., Small M. Complex network from pseudoperiodic time series: Topology versus dynamics. Physical review letters, 2006, 96(23): 238701.  
[9] Lacasa L., Luque B., Ballesteros F., et al. From time series to complex networks: The visibility graph. Proceedings of the National Academy of Sciences, 2008, 105(13): 4972-4975.

- [10] Lacasa L. On the degree distribution of horizontal visibility graphs associated with Markov processes and dynamical systems: diagrammatic and variational approaches. *Nonlinearity*, 2014, 27(9): 2063.
- [11] Luque B., Lacasa L., Ballesteros F., et al. Horizontal visibility graphs: Exact results for random time series. *Physical Review E*, 2009, 80(4): 046103.
- [12] Lacasa L., Toral R. Description of stochastic and chaotic series using visibility graphs. *Physical Review E*, 2010, 82(3): 036120.
- [13] Bezsudnov I. V., Snarskii A. A. From the time series to the complex networks: The parametric natural visibility graph. *Physica A: Statistical Mechanics and its Applications*, 2014, 414: 53-60.
- [14] Gao Z. K., Cai Q., Yang Y. X., et al. Multiscale limited penetrable horizontal visibility graph for analyzing nonlinear time series. *Scientific Reports*, 2016, 6: 35622.
- [15] Xu X., Zhang J., Small M. Superfamily phenomena and motifs of networks induced from time series. *Proceedings of the National Academy of Sciences*, 2008, 105(50): 19601-19605.
- [16] Wang M., Tian L. From time series to complex networks: The phase space coarse graining. *Physica A: Statistical Mechanics and its Applications*, 2016, 461: 456-468.
- [17] Gao X., An H., Fang W., et al. Characteristics of the transmission of autoregressive sub-patterns in financial time series. *Scientific reports*, 2014, 4.
- [18] Gao X., An H., Fang W., et al. Transmission of linear regression patterns between time series: From relationship in time series to complex networks. *Physical Review E*, 2014, 90(1): 012818.
- [19] Wang M., Chen Y., Tian L., et al. Fluctuation behavior analysis of international crude oil and gasoline price based on complex network perspective. *Applied Energy*, 2016, 175: 109-127.
- [20] Chen H., Tian L., Wang M., et al. Analysis of the Dynamic Evolutionary Behavior of American Heating Oil Spot and Futures Price Fluctuation Networks. *Sustainability*, 2017, 9(4): 574.
- [21] Gao Z. K., Yang Y. X., Fang P. C., et al. Multiscale complex network for analyzing experimental multivariate time series. *EPL (Europhysics Letters)*, 2015, 109(3): 30005.
- [22] Gao Z. K., Zhang S. S., Dang W. D., et al. Multilayer Network from Multivariate Time Series for Characterizing Nonlinear Flow Behavior. *International Journal of Bifurcation and Chaos*, 2017, 27(04): 1750059.
- [23] Lacasa L., Nicosia V., Latora V. Network structure of multivariate time series. *Scientific reports*, 2015, 5.
- [24] Wang M., Tian L., Du R.. Research on the interaction patterns among the global crude oil import dependency countries: A complex network approach. *Applied Energy*, 2016, 180: 779-791.
- [25] Du R., Wang Y., Dong G., et al. A complex network perspective on interrelations and evolution features of international oil trade, 2002C2013. *Applied Energy*, 2017, 196: 142-151.
- [26] Wang M., Tian L., Xu H., et al. Systemic risk and spatiotemporal dynamics of the consumer market of China. *Physica A: Statistical Mechanics and its Applications*, 2017, 473: 188-204.
- [27] Wang M., Tian L.. Regulating effect of the energy market!Theoretical and empirical analysis based on a novel energy pricesCeconomy supplyCeconomic growth dynamic system. *Applied Energy*, 2015, 155: 526-546.
- [28] An H., Gao X., Fang W., et al. Research on patterns in the fluctuation of the co-movement between crude oil futures and spot prices: A complex network approach. *Applied Energy*, 2014, 136: 1067-1075.
- [29] Zhou C., Ding L., Skibniewski M. J., et al. Characterizing time series of near-miss accidents in metro construction via complex network theory. *Safety science*, 2017, 98: 145-158.
- [30] Gao Z. K., Hu L. D., Zhou T. T., et al. Limited penetrable visibility graph from two-phase flow for investigating flow pattern dynamics. 2013.
- [31] Grassberger P., Procaccia I. Characterization of strange attractors. *Physical review letters*, 1983, 50(5): 346.
- [32] Sugihara G., Grenfell B., May R. M., et al. Distinguishing error from chaos in ecological time series. *Philosophical Transactions of the Royal Society of London B: Biological Sciences*, 1990, 330(1257): 235-251.

- [33] Kaplan D. T., Glass L. Direct test for determinism in a time series. *Physical review letters*, 1992, 68(4): 427.
- [34] Rosso O. A., Larrondo H. A., Martin M. T., et al. Distinguishing noise from chaos. *Physical review letters*, 2007, 99(15): 154102.
- [35] Kocarev L., Jakimoski G. Logistic map as a block encryption algorithm. *Physics Letters A*, 2001, 289(4): 199-206.
- [36] Gallas J. A. C. Structure of the parameter space of the Hnon map. *Physical Review Letters*, 1993, 70(18): 2714.
- [37] Grigorenko I., Grigorenko E. Chaotic dynamics of the fractional Lorenz system. *Physical review letters*, 2003, 91(3): 034101.
- [38] Panas E., Ninni V. Are oil markets chaotic? A non-linear dynamic analysis. *Energy economics*, 2000, 22(5): 549-568.
- [39] Tabak B. M., Cajueiro D. O. Are the crude oil markets becoming weakly efficient over time? A test for time-varying long-range dependence in prices and volatility. *Energy Economics*, 2007, 29(1): 28-36.